3D Printed Bio-inspired Angular Acceleration Sensor

Joël van Tiem, Jarno Groenesteijn, Remco Sanders and Gijs Krijnen
MESA+ Institute for Nanotechnology, University of Twente, Enschede, THE NETHERLANDS
E-mail: gijs.krijnen@utwente.nl

***Abstract*—We present a biomimetic angular acceleration sensor inspired by the vestibular system, as found e.g. in mammals and fish. The sensor consist of a fluid filled circular channel. When exposed to angular accelerations the fluid flows relative to the channel. Read-out is based on electromagnetic flow sensing (pseudo Hall effect). The sensor is made out of two 3D printed parts which, when put together, form a channel and which allow for easy mounting of permanent magnets and electrodes to measure the flow induced potential difference. Experiments indeed show an acceleration dependent output voltage. However, we find strong contributions from other than electromagnetic sources which, due to their nature and magnitude, are interesting for further research.**

I. Introduction

Despite the maturity and low-cost availability of micro-mechanical rotation-rate sensors based on Coriolis forces, the 3D printed sensors developed in this project are of high interest since they can be easily integrated in (soft) robotic and prosthetic structures, are unaffected by linear accelerations, are rather robust and insensitive to mechanical loading and can potentially be operated at low powers and low voltages compared to resonating structures [1].

In previous work we have shown that the vestibular sensing principle, where angular acceleration is exposed by inertia driven fluid flows, can be used for rotation acceleration sensing. However, that sensor was made by MEMS fabrication technology and used a thermal read-out [2]. The sensor presented here is 3D printed in combination with little assembly anticipating that future printers will allow for fully integrated sensors, customizable on unit-level and low-cost even for single devices.

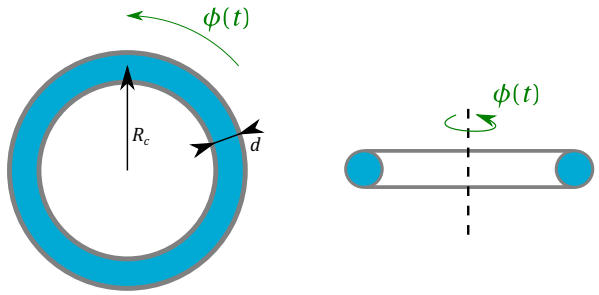

Fig. 1. The 3D printed sensor comprises a fully circular, fluid filled channel. The fluid flow is induced by inertial forces when subjected to an angular acceleration.

II. Theory and Modelling

A. Fluid dynamics

The flow profile inside the channel is governed by the Navier-Stokes equation for incompressible flow [3]:

$$\rho\left(\frac{\partial\vec{v}}{\partial t}+(\vec{v}\cdot\nabla)\vec{v}\right)=-\nabla p+\mu\nabla^2\vec{v}+\vec{f} \tag{1}$$

where $\vec{v}$ denotes the flow velocity, μ the fluid's viscosity, ρ its density and $\vec{f}$ body forces. Because of the fully circular channel we will use cylindrical coordinates to describe the sensor and assume no pressure gradients ($\nabla p = 0$). Furthermore, we assume the velocity to be nonzero only in the direction normal to the channel's cross section (the z-direction) and the channel diameter to be much smaller than the system radius ($d \ll R_c$). The system radius denotes the distance from the center of the channel to the center of the torus. A harmonic angular acceleration with (angular) frequency ω will result in a body force in the axial direction [2]:

$$\vec{f}=\rho R_c\alpha\exp(j\omega t)\ \hat{e}_z \tag{2}$$

in which α denotes the applied (external) angular acceleration and j the imaginary unit. Combining with Equation 1 yields an one dimensional equation describing the flow profile:

$$\mu\left[\frac{\partial^2 v}{\partial r^2}+\frac{1}{r}\frac{\partial v}{\partial r}\right]+\rho R_c\alpha\exp(j\omega t)=\rho\frac{\partial v}{\partial t} \tag{3}$$

which is valid for a Newtonian fluid with a Reynold's number in the fully laminar flow regime ($\rho dv/\mu$ <200) [4]. Imposing the nonslip boundary condition at the wall ($v(d/2,t)=0$) provides a solution for the flow profile within the channel [5]:

$$v(r,t)=-\frac{R_c\alpha}{\omega}\left[1-\frac{J_0\left(r\sqrt{\frac{\omega}{2\nu}}(1-j)\right)}{J_0\left(\frac{d}{2}\sqrt{\frac{\omega}{2\nu}}(1-j)\right)}\right]\exp(j\omega t) \tag{4}$$

in which $\nu=\mu/\rho$ is the kinematic viscosity and J_0 the zeroth order Bessel function. For low frequencies, Equation 3 can be solved by a quasi static expression:

$$v(r,t)=\frac{R_c\alpha}{4\nu}\left(\frac{d^2}{4}-r^2\right)\exp(j\omega t) \tag{5}$$

which is valid only if the frequency is sufficiently low. That is, when the boundary layer thickness δ is larger than the

978-1-4799-8203-5/15/$31.00 ©2015 IEEE

channel's radius ($\delta > d/2$). From Equation 4 it can be observed that δ reads:

$$\delta = \sqrt{\frac{2\nu}{\omega}} \tag{6}$$

Hence we obtain the condition for ω:

$$\omega < \frac{8\nu}{d^2} \tag{7}$$

So the sensor bandwidth benefits from a small channel diameter (d) and a high kinematic viscosity (ν).

B. Electromagnetic flow sensing

If the fluid inside the channel is conductive and a magnetic field is applied normal to the direction of flow, the Lorentz force causes the positive ions to move one way whereas the negative ones will go the other. This charge separation leads to an electric potential which can be measured [6].

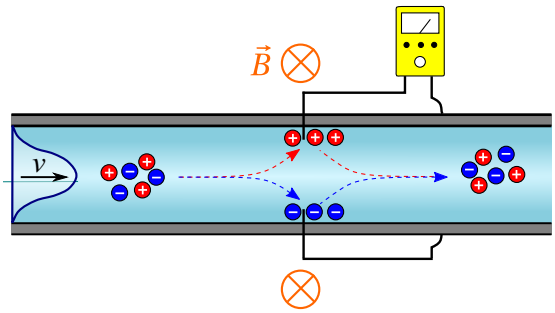

Fig. 2. Illustration of the principle of electromagnetic flow sensing. The magnetic force causes the charges to separate. This separation of charge gives rise to an electric potential.

The total force $\vec{F}_{\text{tot}}$ in equilibrium reads:

$$\vec{F}_{\text{tot}} = q(\vec{E} + \vec{v} \times \vec{B}) = 0 \tag{8}$$

in which q denotes the charge, $\vec{v}$ the flow velocity, $\vec{E}$ the electric field and $\vec{B}$ the applied magnetic field. For a stationary situation the Lorentz force induced by the magnetic field (the $q\vec{v} \times \vec{B}$ term) will be canceled by the one induced by the electric field (the $q\vec{E}$ term) due to the separated charge carriers. If the magnetic field is aligned in such a way that $\vec{v} \perp \vec{B}$, we find:

$$F_{\text{tot}} = q(E + vB) = 0 \rightarrow E = -vB \tag{9}$$

Hence the induced voltage V reads:

$$\begin{aligned} V &= -\int_{\text{L}} \vec{E} \cdot \text{d}\vec{l} \\ &= Ed \\ &= -vBd \end{aligned} \tag{10}$$

in which d is the width of the channel. Note that this expression is valid only for an *uniform* flow profile. This is generally not the case for pipeflow. A more extensive analysis by Shercliff and Kolin demonstrates, however, that Equation 10 is also valid for a non-uniform flow profile, as long as it is symmetrical over the width of the channel, which is the case for pipeflow [7], [8]. We then find:

$$V = -v_{\text{avg}} Bd \tag{11}$$

in which v_{avg} is the average flow velocity over the channel.

So the measured potential difference depends linearly on the flow velocity and therefore on the angular acceleration. This linear relation makes electromagnetic flow sensing an interesting readout mechanism.

Equation 11 is valid only for a constant flow velocity, which is not the case for a harmonically actuated sensor. Two major effects become apparent: the skin effect due to the self inductance and displacement currents. The skin effect can be neglected if the (angular) frequency is sufficiently low compared to the conductivity, magnetic permeability and channel diameter [9], [10]:

$$\omega \ll \frac{2}{\sigma \mu_{\text{m}} d^2} \tag{12}$$

in which σ is the fluid's conductivity and μ_{m} its magnetic permeability. The effects of displacement currents can be neglected if they are much smaller than the conduction current. As described by Shercliff this is the case when the frequency is low compared to the fluid's conductivity and permittivity [7]:

$$\omega \ll \frac{\sigma}{\epsilon} \tag{13}$$

For a fluidic channel with a diameter in the (sub-)millimeter range filled with (tap) water, Equation 7 is, however, the dominant limiting condition on the threshold angular frequency.

III. Design and Fabrication

A key parameter in designing the sensor is the responsivity S. For the angular acceleration sensor, it is defined as

$$S = \frac{\partial V}{\partial \alpha} = \frac{\rho R_{\text{c}} B d^3}{24\mu} \tag{14}$$

So the sensor benefits from a large system radius (R_{c}), a large channel diameter (d), fluids with a low viscosity (μ) and high density (ρ) and magnets with a large magnetic field (B).

The sensor is 3D printed in frosted ultra detail plastic from Shapeways. This technique makes it possible to create engraved, rectangularly shaped channels of minimally $100 \times 100\,\mu\text{m}$. The channel should be as low as possible for two reasons. First, in this fashion the permanent magnets are as close as they can get, hence maximizing the magnetic field inside the channel. Second, the smaller the channel, the higher the threshold frequency (refer to Equation 7). If the height of the channel is small, the width should be large to maintain a high responsivity.

The sensor is fabricated from two separately 3D printed parts with predefined room for the permanent magnets of approximately $250\,\mathrm{mT}$ each (Supermagnete) and trenches for the electrodes. Alignment markers on the bottom and top parts ensure proper alignment. The platinum electrodes and the two 3D printed parts are assembled and fixated by UV sensitive glue.

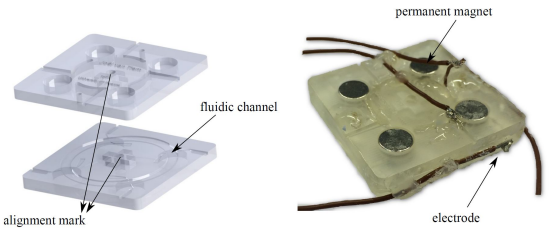

Fig. 3. Design of the two separately 3D printed parts (left) and the assembled sensor (right).

Apart from the angular acceleration sensor, a straight channel configuration, which is actuated by means of a flow controller, has been designed as well.

Fig. 4. The design of the straight channel is very similar to the angular acceleration sensor. However, here the flow is applied by an external flow controller rather than an angular acceleration.

IV. Experimental

A. Angular acceleration sensor

The angular acceleration sensor is mounted to an in-house built rotation table, which is able to actuate the sensor harmonically. The frequency of rotation is set by a function generator. The amplitude of this rotation (and hence the magnitude of the applied angular acceleration) is determined by measuring the width of a laser beam projected on a flat sheet next to the rotation table.

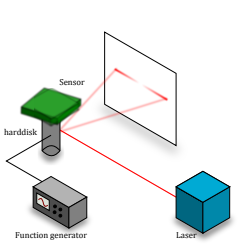

(a) Illustration of the setup.

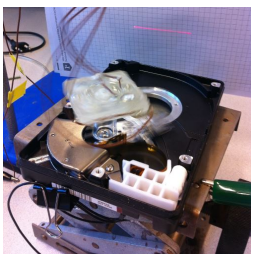

(b) The angularly accelerated sensor.

Fig. 5. The setup used to characterize the angular acceleration sensor. By measuring the width of the projected laser beam and the sensor-screen distance the amplitude of angular acceleration is determined.

A lowpass filter (Stanford Research System Model SR650) has been set to $30\,\mathrm{Hz}$ and an output gain of $20\,\mathrm{dB}$. Next, the voltage was measured by a multimeter (HP34401A). The sensor's channel has a cross section of $0.4 \times 3\,\mathrm{mm}$ and the system radius measures $15\,\mathrm{mm}$. The measurements are performed with tap water (σ=$450\,\mu\mathrm{S\,cm^{-1}}$) at room temperature. The results are shown in Figure 6.

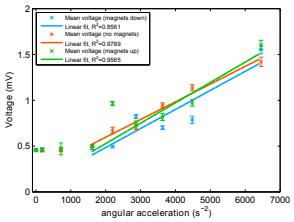

(a) Voltage as a function of angular acceleration.

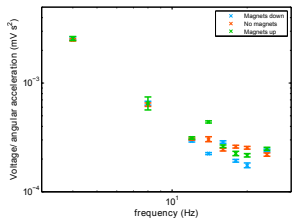

(b) Log-log plot for the normalized voltage as a function of frequency.

Fig. 6. Measured voltages as a function of angular acceleration for magnets up, down and without magnets. A linear fit through the data points has been made. In this fit the anomaly at $16\,\mathrm{Hz}$ for magnets up (approximately $2200\,\mathrm{s^{-2}}$) has not been taken into account.

The measurements have been performed with the magnetic field pointed in one and the opposite direction, and without a magnetic field at all, see Figure 6(a). Above an angular acceleration of approximately $1500\,\mathrm{s^{-2}}$ the output voltage increases clearly with angular acceleration. However, from Figure 6(b) we also conclude that there is a low pass behavior which is not associated with the electromagnetic readout.

B. Straight channel

The potential induced by the magnetic field is not necessarily the only source of electrical potential in the sensor output. Among others, inductive coupling, the streaming potential and an electrochemical reaction can give rise to electrical potentials as well [11]. In order to counteract these effects, the potential is measured differentially. In theory this will double the signal induced by the magnetic field and cancel other potentials:

$$V = \underbrace{(V_{\mathrm{magn}} + V_{\mathrm{other}})}_{V_1} + \underbrace{(V_{\mathrm{magn}} - V_{\mathrm{other}})}_{V_2} = 2V_{\mathrm{magn}} \qquad (15)$$

where V denotes the *measured* potential. The principle is illustrated in Figure 7.

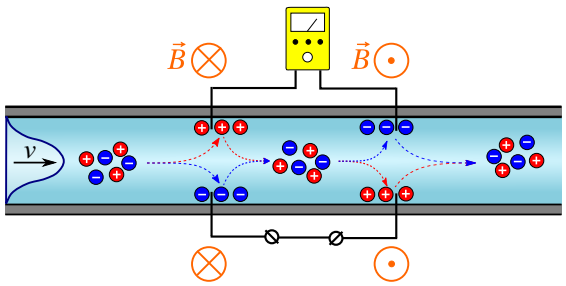

Fig. 7. Measuring differentially amplifies the potential induced by the magnetic field whereas it cancels a potential induced by an other source.

The flow controller (PHD Ultra) applies a flow ranging from $900\,\mathrm{mL\,h^{-1}}$ infusing to $900\,\mathrm{mL\,h^{-1}}$ withdrawing with steps of $300\,\mathrm{mL\,h^{-1}}$. Given the channel cross sectional area, this translates to a flow velocity of $\pm 208\,\mathrm{mm\,s^{-1}}$ in steps of $69\,\mathrm{mm\,s^{-1}}$. This cycle is repeated three times. The control measurement is performed using a commercial flow meter (Bronkhorst mini CORI-FLOW M14). The results are shown in Figure 8.

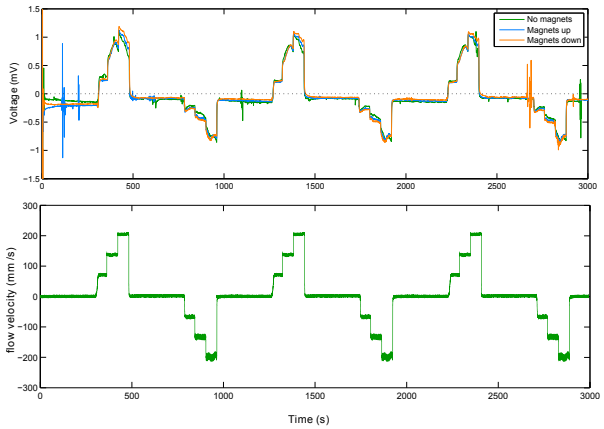

Fig. 8. Top: the measured voltage for the sensor with no magnets applied to it (green), the magnetic field oriented in one direction (blue) and in the other direction (orange). Bottom: the applied flow profile as measured externally in the control experiment.

Similar to the measurements performed with the angular acceleration sensor, there is a strong non-magnetic effect that gives rise to a flow dependent potential. To further investigate this effect the flow response was measured for water solutions with various conductivities (deionized water, tap water and salt water with 11, 450 and $2900\,\mu\mathrm{S\,cm^{-1}}$, respectively) *without* a magnetic field applied. The results are shown in Figure 9.

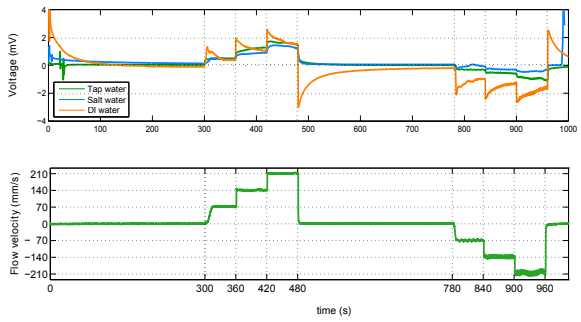

Fig. 9. Measurements on the straight channel without a magnetic field applied to it. The signal depends on the solution used.

Even without magnets there is an appreciable signal, which is dependent on the solution used, with increasing time-constant for decreasing conductivity, but strongly related with the fluid flow. Hence this is an alternative way of measuring fluid flows and potentially usable for the angular acceleration sensor.

V. Discussion

The effect of electromagnetic readout is not clearly observed. The signal does not change significantly when opposing the direction of the magnetic field or even removing the external magnetic field. In addition, measuring differentially does not cancel the undesired effects.

A plausible cause of the measured potential could be the streaming potential, which is induced by surface charge at the channel wall. It depends on both the flow velocity and the fluid conductivity and the measured potential is in the same order of magnitude as could be expected from theory [11], [12].

VI. Conclusion

We have presented a 3D printed angular acceleration sensor with intended electro-magnetic read-out. Measurements have shown that other effects play an important role in the generation of the output signal. Current research is aimed at improving our understanding of the observed effects.

Acknowledgment

This research is being carried out within the Coriolis Based SAS project of NanoNext NL. Contributions from Jan Eijkel have been valuable.

References

[1] C. M. Andreou, Y. Pahitas, and J. Georgiou, "Bio-inspired micro-fluidic angular-rate sensor for vestibular prostheses," *Sensors*, vol. 14, no. 7, pp. 13 173–13 185, 2014.

[2] J. Groenesteijn, H. Droogendijk, M. de Boer, R. Sanders, R. Wiegerink, and G. Krijnen, "An angular acceleration sensor inspired by the vestibular system with a fully circular fluid-channel and thermal read-out," 2014.

[3] B. R. Munson, D. F. Young, and T. H. Okiishi, *Fundamentals of fluid mechanics*. New York, 1990.

[4] X. Peng, G. Peterson, and B. Wang, "Frictional flow characteristics of water flowing through rectangular microchannels," *EXPERIMENTAL HEAT TRANSFER An International Journal*, vol. 7, no. 4, pp. 249–264, 1994.

[5] H. Schlichting, "Boundary-layer theory," 1968.

[6] H. Yoon, S. Kim, S. Lee, and S. S. Yang, "Fabrication of a microelectromagnetic flow sensor for microflow rate measurement," in *SPIE's 7th Annual International Symposium on Smart Structures and Materials*. International Society for Optics and Photonics, 2000, pp. 264–271.

[7] J. A. Shercliff, *The theory of electromagnetic flow-measurement*. CUP Archive, 1962.

[8] A. Kolin, "An alternating field induction flow meter of high sensitivity," *Review of Scientific Instruments*, vol. 16, no. 5, pp. 109–116, 1945.

[9] D. Mattis and J. Bardeen, "Theory of the anomalous skin effect in normal and superconducting metals," *Physical Review*, vol. 111, no. 2, p. 412, 1958.

[10] H. A. Wheeler, "Formulas for the skin effect," *Proceedings of the IRE*, vol. 30, no. 9, pp. 412–424, 1942.

[11] W. Olthuis, B. Schippers, J. Eijkel, and A. van den Berg, "Energy from streaming current and potential," *Sensors and Actuators B: Chemical*, vol. 111, pp. 385–389, 2005.

[12] Y. Gu and D. Li, "The ζ-potential of glass surface in contact with aqueous solutions," *Journal of Colloid and Interface Science*, vol. 226, no. 2, pp. 328–339, 2000.